

Semiconductor laser under resonant feedback from a Fabry-Perot resonator: Stability of continuous-wave operation

V. Z. Tronciu

Department of Physics, Technical University of Moldova, Stefan cel Mare av. 168, Chisinau MD-2004, Republic of Moldova

H.-J. Wünsche

Institute of Physics, Humboldt-University Berlin, Newtonstr. 15, 12489 Berlin, Germany

M. Wolfrum and M. Radziunas

Weierstraß-Institut für Angewandte Analysis und Stochastik, Mohrenstraße 39, 10117 Berlin, Germany

(Received 3 August 2005; published 18 April 2006)

We study the continuous-wave (cw) operation of a semiconductor laser subject to optical feedback from a Fabry-Perot resonator in a case where the emission is resonant to a reflection minimum of the resonator. This configuration is treated in the framework of Lang-Kobayashi equations. The nature of bifurcations and the stability of steady state solutions is analyzed in terms of the dependence on magnitude and phase of the feedback. In contrast to conventional optical feedback from a single mirror, the locus of external cavity modes is not elliptic but represents a tilted eight with possible satellite bubbles. Below a critical feedback strength, which is analytically given, only one single mode exists representing the completely unchanged cw emission of the laser. In this weak-feedback regime, the feedback phase allows noninvasive control of the cw emission and a tailoring of its small-signal response within wide limits. The results obtained are a prototype for all-optical realizations of delayed feedback control.

DOI: [10.1103/PhysRevE.73.046205](https://doi.org/10.1103/PhysRevE.73.046205)

PACS number(s): 05.45.-a, 42.65.Sf, 42.55.Px, 42.60.Da

I. INTRODUCTION

Stabilization of laser emission by external cavities is long established [1–4] and of continuous interest [5,6]. Fabry-Perot (FP) cavities are mostly operated as optical filters, which suppress all waves which do not fit in the narrow spectral resonances [3–5]. The only exception, to our knowledge, is the powerful Pound-Drever-Hall technique [2], which exploits a resonant minimum of the FP reflectivity in order to derive an electronic control signal used to lock the laser cavity to the FP resonance.

In contrast to all these methods, we consider stability control by direct optical feedback from an FP with mirror-reflectivity R and round trip time τ_{FP} (Fig. 1). Under ideal conditions, in particular no loss and equal phase and group velocities, the feedback field is

$$\mathcal{E}_b(t) = K \sum_{n=0}^{\infty} R^n \cdot [\mathcal{E}(t_n) - \mathcal{E}(t_n - \tau_{\text{FP}})]. \quad (1)$$

$\mathcal{E}(t)$ represents the field amplitude emitted by the laser. $t_n = t - \tau_l - n\tau_{\text{FP}}$ is delayed by n round trips in the resonator plus the round trip time τ_l between laser and resonator. K measures the magnitude of feedback, including a possible attenuation between FP and laser.

We focus on a case where the laser without feedback is assumed to emit continuous wave (cw) with a single frequency ω_0 resonant to the FP, i.e., $\omega_0\tau_{\text{FP}}$ is an integer multiple of 2π . In this particular case, \mathcal{E} is τ_{FP} -periodic and the feedback field \mathcal{E}_b becomes zero. Thus, the free running state of the laser is not modified by the presence of the resonant FP. One might wonder whether the resonator has any influ-

ence at all. However, perturbations and noise cause deviations from the ideal state giving rise to a nonzero feedback, which in turn modifies the response of the laser to the perturbations. Thus, the considered feedback configuration does not change the laser state itself but its stability properties.

Delayed feedback of type (1), originally introduced by Pyragas and Socolar [7–9], is well known as a general and self-adaptive method for noninvasive control of dynamical systems. Delayed-feedback control (DFC) has been widely used to stabilize unstable periodic orbits within chaos [7–10]. It is also able to improve the coherence of oscillatory motion under the impact of noise [11,12]. Very recently, DFC has successfully been used to control the stability of equilibria [13].

Already one decade ago, Socolar *et al.* [8,9] noticed that feedback from a FP should allow an all-optical implementation of this general control scheme. Surprisingly, no in-depth study of such an implementation exists until now, although the first numerical explorations [14–16] of similar interferometric configurations gave examples for the possibility of an all-optical chaos control. The lack of progress is supposedly related to the multiple time scales being specific for all-optical configurations [14]. They range over more than six orders of magnitude from the femtoseconds of the optical oscillations over hundreds of picoseconds for inversion oscillations up to round-trip cycles of several nanoseconds in the long-cavity configurations considered in Refs. [14–16]. In contrast to other applications of the Pyragas-Socolar schema, oscillations on longer time scales are to be controlled here with an interferometric feedback that is sensitive to the shorter time scales, too. Indeed, using the standard scaling $\mathcal{E}(t) = \text{Re}\{E(t)\exp(i\omega_0 t)\}$ onto slowly varying amplitudes $E(t)$, Eq. (1) transforms to

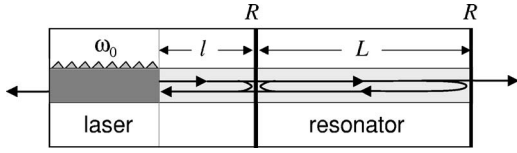


FIG. 1. Schematic view of a single-mode DFB laser coupled to a Fabry-Perot resonator. R , mirror reflectivity; L , resonator length; l , distance between laser and resonator. Due to the finite group velocity c_g , the geometry causes two time delays, the round trip times $\tau_{FP}=2L/c_g$ and $\tau_l=2l/c_g$ within the FP and between laser and FP, respectively.

$$E_b(t) = \mathcal{K} \sum_{n=0}^{\infty} \mathcal{R}^n [E(t_n) - e^{-i\phi} E(t_n - \tau_{FP})], \quad (2)$$

with $\mathcal{K}=Ke^{-i\varphi}$ and $\mathcal{R}=Re^{-i\phi}$. This differs from the conventional Pyragas-Socolar feedback by being complex valued and by the presence of the two optical phase shifts $\varphi=\omega_0\tau_l$ and $\phi=\omega_0\tau_{FP}$. If phase and group velocities differ from each other, $\varphi=2l\omega_0/c_p$ and $\phi=2L\omega_0/c_p$ are governed by the phase velocity c_p , in contrast to the round-trip times $\tau_l=2l/c_g$ and $\tau_{FP}=2L/c_g$, which are determined by the group velocity c_g . Incorporation of possible phase shifts by the mirrors is also straightforward.

Obviously, the impact of this control term depends sensitively on both phases. This very fact opens new degrees of freedom for tailoring the feedback control but it also requires the mastery of the geometry of the configuration on length scales small compared to the wavelength. Fortunately, continuing technological progress of multi-section lasers (see, e.g., Ref. [17]) brings into reach correspondingly stable configurations (Fig. 1) with integrated common waveguides and with phase shifts tunable by injection currents.

The present paper represents a first theoretical study of such a configuration. In view of the complexity of the problem, we restrict the analysis to the simplest nontrivial case, a single-mode laser with stable continuous-wave (cw) emission being resonant to the FP, i.e., $\phi \bmod 2\pi=0$. Regarding cw emission as spiral point of the rate equations for photon number and inversion, this case seems simply to correspond to delayed-feedback control of the equilibrium of an dissipative oscillator studied already in Ref. [13]. However, coherent optical feedback (2) cannot be incorporated into photon-number equations and the present analysis will reveal a higher complexity compared to Ref. [13]. We expect a similar increase of complexity when going from conventional to all-optical delayed-feedback stabilization of periodic oscillations. An explicit treatment of the latter case is, however, beyond the scope of the present paper.

The following analysis based on the well-known Lang-Kobayashi equations [18], generalized to feedback of type (2), which are introduced in Sec. II. Having integrated devices in mind, a short FP cavity is considered with small reflectivity R , allowing the neglect of multiple reflections. Analytic equations are derived in Sec. III for the external cavity modes (ECM) and evaluated for an example set of parameters. In Sec. IV, we focus on the bifurcations introduced by the resonant feedback from the FP and on its im-

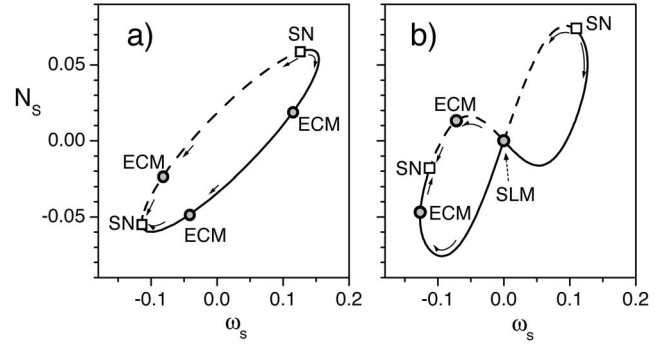


FIG. 2. Curves of ECMs in the (ω, N) plane for $K=0.05$. (a) Conventional optical feedback. (b) Resonant feedback from Fabry-Perot cavity. SN, Saddle-node bifurcation. ECM, External cavity mode at a particular feedback phase. SLM, Solitary laser mode. Solid line, Node. Dashedline, Saddle. Arrows indicate how the ECM move with increasing feedback phase. SLM keeps its position independent of phase.

act on the local and global stability of laser states. Feedback strength K and phase φ are considered as main bifurcation parameters. The particular impact of the Fabry-Perot on frequency and damping of relaxation oscillation is evaluated in Sec. V. Finally, conclusions are drawn in Sec. VI.

II. MODEL AND EQUATIONS

In this section we will discuss the laser setup and a model for a single mode DFB laser under the influence of a resonant feedback from a Fabry-Perot resonator (RFFP). Such a configuration is shown schematically in Fig. 1. We will use a Lang-Kobayashi type system [18] for the complex field amplitude E and an excess carrier density N . In dimensionless form, it is given by [19]

$$\frac{dE}{dt} = (1 + i\alpha)NE + E_b(t), \quad (3)$$

$$\frac{dN}{dt} = \frac{1}{T}[J - N - (2N + 1)|E|^2], \quad (4)$$

where J is an excess pump current, T is the ratio of the carrier lifetime, and the photon lifetime, and α is the line-width enhancement factor. The time is measured in units of photon lifetime.

As mentioned above, we focus on the resonant case $\phi=0$, i.e., the cw emission of the unperturbed laser is at a minimum of the FP reflectivity. Additionally we assume a small reflectivity $R \ll 1$ and account only for one round trip in the air gap and in the Fabry-Perot cavity. In this case the feedback term can be written as

$$E_b(t) = Ke^{-i\varphi}[E(t - \tau_l) - E(t - \tau)], \quad (5)$$

where $\tau=\tau_l+\tau_{FP}$. Note that K is also rescaled by choosing the nondimensional LK model.

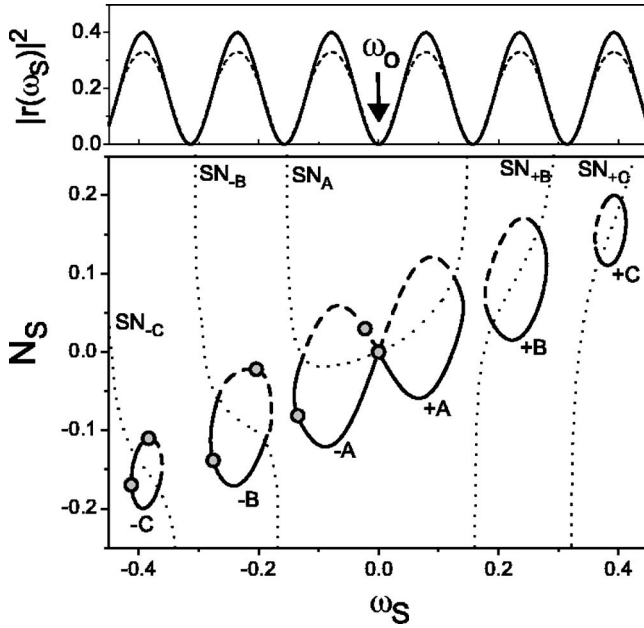


FIG. 3. Top panel, Reflection spectrum of a Fabry Perot resonator with mirror reflectivity $R=0.1$. Solid line, $n=0$ contribution of Eq. (2). Dashedline, including all multiple round-trips in the resonator. Arrow, resonant position of the solitary laser frequency ω_0 . Lower panel, Location of ECMs of systems (3)–(5) for $K=0.1$. Circles, ECMs for fixed $\varphi=0$. Dottedline, Saddle-node curves (SN) separating between modes and antimodes.

III. EXTERNAL CAVITY MODES (ECM)

We begin our analysis by studying stationary lasing states of systems (3)–(5). They are given by rotating wave solutions of the form

$$E(t) = E_S e^{i\omega_S t}, \quad N = N_S, \quad (6)$$

which are usually called the external cavity modes (ECMs). Inserting (6) into (3) and splitting the equation into real and imaginary parts, we obtain

$$N_S = K[-\cos(\varphi + \omega_S \tau_l) + \cos(\varphi + \omega_S \tau)], \quad (7)$$

$$\omega_S - \alpha N_S = K[-\sin(\varphi + \omega_S \tau_l) + \sin(\varphi + \omega_S \tau)]. \quad (8)$$

The carrier equation (4) can be used to obtain the output intensity

$$|E_S|^2 = \frac{J - N_S}{2N_S + 1}. \quad (9)$$

Finally, inserting (7) into (8), we obtain

$$\omega_S = \alpha K[\cos(\varphi + \omega_S \tau) - \cos(\varphi + \omega_S \tau_l)] + K[\sin(\varphi + \omega_S \tau) - \sin(\varphi + \omega_S \tau_l)]. \quad (10)$$

Note that the equations for ECMs of a laser with simple optical feedback (see, e.g., [20]) can be obtained from (7)–(10) by just dropping all terms containing τ_l . In this case it is well known that in the (ω, N) plane, the ECMs are located on ellipses. For feedback

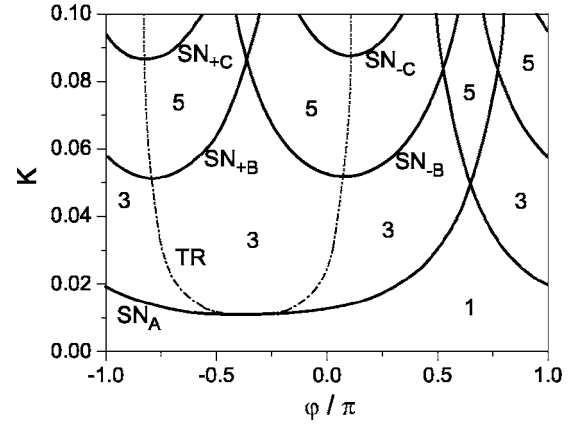


FIG. 4. Lines of saddle-node (SN) and transcritical (TR) bifurcations at different locations; number of ECMs in corresponding regions

$$K < \frac{1}{\tau\sqrt{1 + \alpha^2}},$$

there is only one ECM, moving along the ellipse for varying phase φ . For feedback strength K above this critical value, larger numbers of ECMs appear with increasing K . Varying φ , they appear and disappear in pairs at saddle-node bifurcations at the top and the bottom end of the ellipse [see Fig. 2(a), or [20] for more details].

In contrast to this situation, we always have for RFFP an ECM at the origin, which we denote as solitary laser mode. This is due to the fact that at resonance the CW emission of the laser does not get any feedback. However, as we will see later, its stability properties will change drastically. Below the critical feedback level

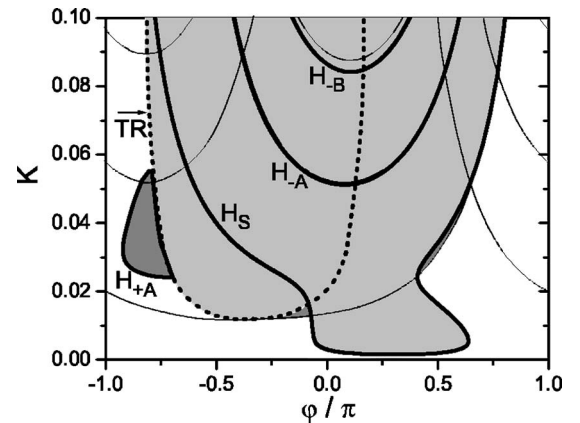


FIG. 5. Hopf bifurcations of stable ECMs at different locations (thick solid): Solitary laser mode (H_S), ECMs on the right (H_{+A}) and left (H_{-A}) part of the figure eight, and on satellites (H_{+B} , H_{-B}). Stability of the central mode. White area, CW operation. Light-gray region, unstable regime of central mode. Dark-gray regions, bistability between central and first modes. Thick dotted line, Transcritical bifurcation. Thin solid line, saddle-node bifurcation.

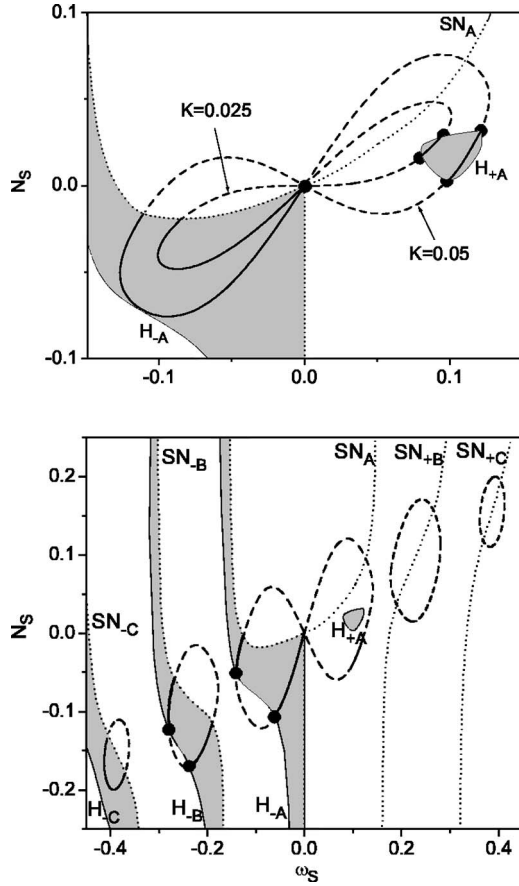


FIG. 6. Region of stable ECMs in the (N_S, ω_S) plane (shaded), bounded by lines of Hopf bifurcations (thin solid) and saddle-node bifurcations (dotted). Upper panel, With figure of eight for $K=0.025$ and $K=0.05$. Lower panel, with figure of eight and satellite bubbles for $K=0.1$. Thick solid line Location of stable ECMs. Thick dashed line, location of unstable ECMs. Full circles, Hopf bifurcation points for fixed values of K . Labels as in Fig. 3.

$$K_c = \frac{1}{\tau_{FP} \sqrt{1 + \alpha^2}}, \quad (11)$$

there can exist only the solitary laser mode. For larger feedback, additional ECMs can appear again in pairs at saddle-node bifurcations. For varying phase φ they now move along a figure eight, meeting the solitary laser mode, which is sitting in the waist, at transcritical bifurcations [see Fig. 2(b)]. For larger values of K , additional to the figure eight there appear satellite bubbles of ECM locations, located around neighboring reflectivity maxima of the FP resonator, see Fig. 3. Differentiating (10), we obtain the condition for saddle-node bifurcations:

$$1 = K[\alpha\tau_1 \sin(\varphi + \omega_S\tau_1) - \alpha\tau \sin(\varphi + \omega_S\tau) - \tau_1 \cos(\varphi + \omega_S\tau_1) + \tau \cos(\varphi + \omega_S\tau)] \quad (12)$$

This equation together with the ECM conditions (7) and (8) can now be solved numerically. We fixed the parameters

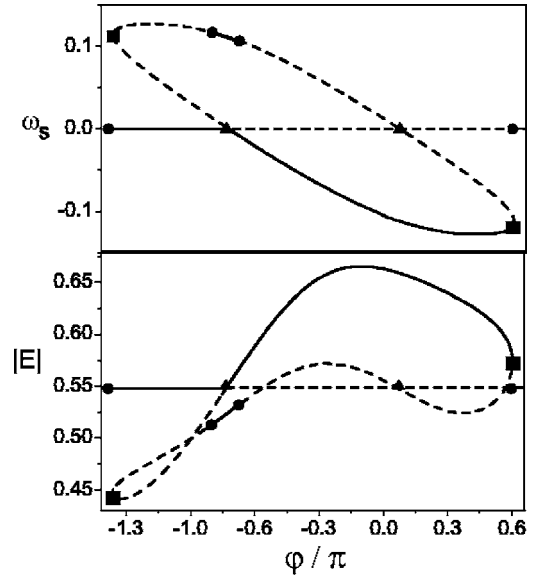


FIG. 7. Bifurcation diagrams for $K=0.05$. Upper panel, (ω_S, φ) plane. Lower panel, $(|E|, \varphi)$ plane. Transcritical and Hopf bifurcations are marked by triangles and circles, respectively. Solid lines, stable stationary solutions; dashed lines, unstable ones. Squares, Saddle-node bifurcations.

$$\alpha = 2, \quad J = 0.3, \quad T = 1000, \quad \tau_l = 0.001, \quad \tau_{FP} = 40, \quad (13)$$

and varied feedback strength K and phase φ . In the lower part of Fig. 3, we show the situation in the (ω, N) -plane: The saddle-node curves separate the ECMs on the figure eight and their satellites in saddles and nodes. They are usually called antimodes and modes, respectively. The antimodes (dashed) are always unstable, the modes (solid) are stable until they destabilize in a Hopf bifurcation, which we discuss in the next section. Figure 4 shows the corresponding bifurcation scenario in the plane of the feedback parameters K and φ . Additional ECMs appear on the figure of eight at the curve of saddle-node bifurcations SN_A . On the satellites $(+B, -B, +C, -C, \dots)$, the corresponding bifurcation curves are $SN_{+B}, SN_{-B}, SN_{+C}, SN_{-C}, \dots$. At the transcritical bifurcation line TR , ECMs move from the left part $+A$ of the figure eight to the right part $-A$. Note that the degenerate point, where the transcritical bifurcation meets the saddle-node, represents a codimension 3 bifurcation, which is not completely unfolded here since we have fixed the resonance condition.

IV. STABILITY OF ECMS

In the following we use the software DDE-BIFTOOL [21] to study the stability properties of the ECM solutions discussed above. To this end, it is necessary to use the ECM frequency as a reference frequency, which transforms the rotating wave into a stationary solution. In this way, ω_S is considered as an extra free parameter. To exclude the degeneracy originating from the phase shift invariance, one has to induce an additional constraint, e.g., $\text{Re}(E_S) = 0$. It turns out that there are

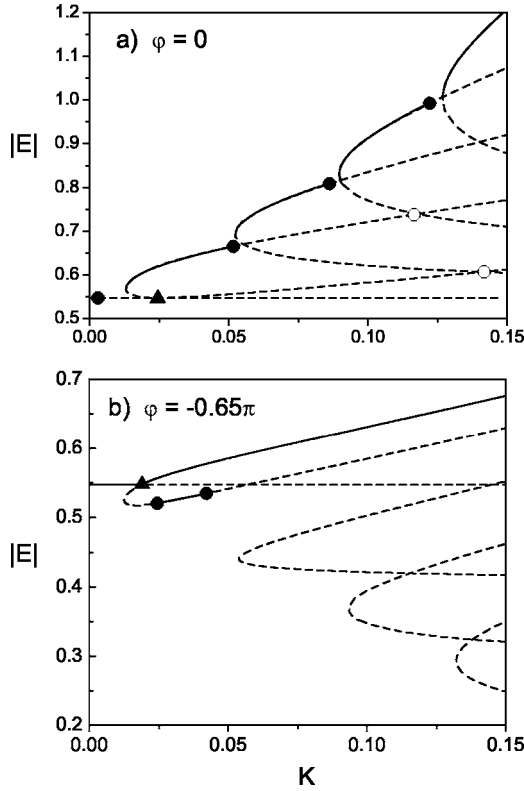


FIG. 8. Bifurcation diagram of the steady states in the plane $|E|$ vs the feedback strength K for $\varphi=0$ and $\varphi=-0.65\pi$. The solid lines show the stable stationary solutions. Circles indicate the Hopf bifurcation points. The empty circles denote the Hopf-bifurcation which appears on unstable branches. The triangle denotes transcritical bifurcation.

three different possibilities for Hopf bifurcations of stable ECMs (see Fig. 5).

The solitary laser mode in the waist of the figure of eight can become unstable in a Hopf bifurcation (H_S). This can happen even for feedback $K < K_c$, where the solitary laser mode is the only existing ECM.

On the left part $-A$ of the figure of eight and on the left satellites ($-B, -C, \dots$), stable ECMs originate from the saddle-node bifurcation. They can become unstable for further increasing φ at the corresponding Hopf curves H_{-A}, H_{-B}, \dots . This happens only for a sufficiently large feedback level K .

On the right part $+A$ of the figure of eight and on the right satellites ($+B, +C, \dots$), all ECMs are unstable, in general. Only in a small island on $+A$, bounded by the Hopf curve H_{+A} , they are stable.

The location of stable ECMs in the (ω, N) plane is given by the shaded region in Fig. 6. Note that the vertical line at $\omega_S=0, N < 0$ is not a bifurcation curve, because, as at the other reflectivity minima of the resonator, ECMs do not exist there. Only in the limit of infinite K do ECMs approach this line.

Figure 7 shows a specific bifurcation scenario for fixed $K=0.05$. Figure 8 resembles the situations φ fixed to 0 and -0.65π . Note that for $\varphi=0$, the solitary laser mode destabilizes already for very small values of K . Collecting all bifur-

cations of the solitary laser mode, we can determine its stability region. In Fig. 5, the region of instability of the solitary laser mode is shaded in light gray. In dark grey, we indicated regions of coexistence with another stable ECM (bistability). For large feedback, there might exist other stable objects (e.g., periodic solutions) which we have not captured in our calculations.

As one expects from optical feedback, the feedback phase has a decisive role, whether the feedback acts to stabilize or destabilize the solitary laser mode. In the next section we perform a detailed study on the linear stability properties of the solitary laser mode.

V. RELAXATION OSCILLATIONS

Now we consider the control of relaxation oscillations by the resonator. To this purpose, system (3)–(5) is linearized in the form

$$\frac{d}{dt} \mathbf{v}(t) = A \mathbf{v}(t) + B \mathbf{v}(t - \tau_l) + C \mathbf{v}(t - \tau), \quad (14)$$

where $\mathbf{v}(t) = (\text{Re } E(t) - E_1, \text{Im } E(t) - E_2, N(t) - N_S)$ represents the deviation from field $E_S = E_1 + iE_2$ and carrier density N_S of a selected ECM. The matrices A , B , and C are

$$A = \begin{pmatrix} N_S & \omega_S - \alpha N_S & E_1 - \alpha E_2 \\ \alpha N_S - \omega_S & N_S & E_2 + \alpha E_1 \\ -2E_1 G/T & -2E_2 G/T & -(1 + 2|E_S|^2)/T \end{pmatrix},$$

$$B = K \begin{pmatrix} \cos(\varphi_S) & \sin(\varphi_S) & 0 \\ -\sin(\varphi_S) & \cos(\varphi_S) & 0 \\ 0 & 0 & 0 \end{pmatrix},$$

$$C = -K \begin{pmatrix} \cos(\phi_S) & \sin(\phi_S) & 0 \\ -\sin(\phi_S) & \cos(\phi_S) & 0 \\ 0 & 0 & 0 \end{pmatrix},$$

with $G = 1 + 2N_S$, $\varphi_S = \varphi + \omega_S \tau_l$, and $\phi_S = \phi + \omega_S \tau$ being gain and optical phase shifts, respectively, in the considered stationary state. The characteristic equation for eigenvalues of this linear system has the form

$$\chi(\lambda) = \det(\lambda E - A - e^{-\lambda \tau_l} B - e^{-\lambda \tau} C) = 0, \quad (15)$$

which determines the complex parameter λ . The real and imaginary parts of $-\lambda$ correspond in general to decay rates γ and oscillation frequencies ω , respectively, of small deviations from the ECM.

In the special case of a solitary laser, one has $K=0$, $N_S=0$, $\omega_S=0$ and $|E_S|^2=J$ and one gets the known expressions for damping and frequency of relaxation oscillations (RO), which are $\gamma = (1 + 2J)/2T$ and $\omega = \sqrt{2J/T}$, respectively, in lowest order of $1/T$. These quantities determine important parameters of lasers like small signal response, relative intensity noise (RIN), and chirp (see, e.g., chapter 6 of Ref. [22]). of the system.

To highlight control of these properties by the resonator, we have calculated the nonzero roots of Eq. (15) for the

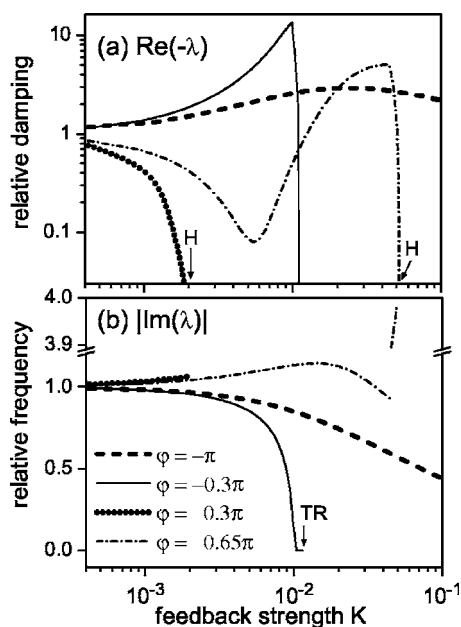


FIG. 9. Solutions λ of the characteristic equation (15) for the central mode vs feedback strength K . Only the respective solution with highest $\text{Re } \lambda < 0$ is shown. (a) $\gamma = -\text{Re } \lambda$ and (b) $\omega = |\text{Im } \lambda|$ correspond to damping and frequency of relaxation oscillations, respectively. H and TR label Hopf and transcritical bifurcations, respectively. The curves are normalized to the values without feedback. Parameters, Eq. (13).

central mode in dependence on feedback strength K and phase φ . Plots of λ versus K are shown in Fig. 9 for some particular phases φ representing the different regions in Fig. 5. Note that $\varphi = \pm\pi$ corresponds to conventional delayed feedback as used to control steady states in Ref. [13]. In accordance with those results, the solitary laser mode becomes more stable here, showing enhanced damping and reduced frequency of relaxation oscillations (thick dashed in Fig. 9). At $\varphi = 0.3\pi$ (thick dotted), the RO-damping drops rapidly down towards the Hopf bifurcation H at $K \approx 0.002$. The frequency variation is negligible in this tiny interval. A transition from weak damping to overdamping is manifested in the case $\varphi = -0.3\pi$ (solid). The decay rate first increases with K , passes a kink, and then falls dramatically towards the transcritical bifurcation TR. At the kink, the frequency goes to zero and the damping is enhanced by more than one order of magnitude. Perturbations decay rapidly (within few tens) and monotonically in this regime. Such behavior is possibly of great interest for high-speed laser modulation. A similar high damping with a kink and subsequent sudden decrease appears also for $\varphi = 0.65\pi$ (dash-dotted) just before the Hopf bifurcation H. As before, this scenario is related to the proximity of a saddle-node bifurcation of two other ECM

(cf. Fig. 5). However, the frequency keeps finite here and it even jumps to much higher values beyond the kink. The dip in the damping around $K \approx 0.005$ is caused by the influence of the nearby Hopf bifurcation curve H_S , see Fig. 5. Altogether, these examples demonstrate interesting possibilities for controlling the small-signal dynamics of a laser without changing its CW output.

VI. CONCLUSION

In the framework of properly adapted Lang-Kobayashi equations, we have treated a single-mode semiconductor laser under resonant optical feedback from a Fabry-Perot cavity. Evaluation of mode spectra and of the most relevant bifurcations in dependence of magnitude and phase of the feedback leads to a comprehensive picture. Below a critical feedback strength K_c , analytically given in Eq. (11), only one single mode exists. This represents the completely unchanged CW emission of the laser. Although the solitary laser mode is unmodified by the resonator, the stability changes drastically. The effects range from destabilization of relaxation oscillations in Hopf bifurcations to transitions into overdamped behavior, in sensitive dependence on the feedback phase. Thus, this weak-feedback regime allows wide control of the small-signal performance of the laser without feedback-induced changes of the laser state. If the feedback exceeds K_c , an increasing number of additional external cavity modes (ECM) appear as mode-antimode pairs in saddle-node bifurcations. Transcritical bifurcations as well as multistability reduce the local and global stability of the solitary laser mode in this regime.

The results obtained are a prototype for all-optical realizations of delayed feedback control (DFC). The optical phase generally appears as a new control parameter, which is not present in standard DFC. Maximum stability against perturbations has been obtained at a feedback phase different from π that corresponds to standard DFC. The round-trip phase shift in the FP must equal an integer multiple of 2π in order to get noninvasive control. In addition, for an attempted noninvasive stabilization of periodic intensity-pulsations, the group round-trip time will have to match the pulsation period. Our result on the critical feedback strength K_c , above which feedback-induced modes may prevent stabilization of CW emission, will also remain valid for an all-optical DFC of other target states.

ACKNOWLEDGMENTS

V.Z.T. acknowledges AvH and Royal Society for support and expresses his gratitude for the hospitality in the “Laser Dynamics” group at WIAS and Photonik at HUB. This work was supported by Deutsche Forschungsgemeinschaft within Sfb 555 and Research Center “Matheon.”

- [1] R. F. Kazarinov and Ch. H. Henry, *IEEE J. Quantum Electron.* **23**(9), 1401 (1987).
- [2] R. W. P. Drever *et al.*, *Appl. Phys. B* **31**(2), 97 (1983).
- [3] B. Dahmani, L. Hollberg, and R. Drullinger, *Opt. Lett.* **12**(11), 876 (1987).
- [4] C. E. Wieman and L. Hollberg, *Rev. Sci. Instrum.* **62**(1), 1 (1991).
- [5] V. V. Vassiliev, S. M. Il'ina, and V. L. Velichansky, *Appl. Phys. B* **76**, 521 (2003).
- [6] Kenji Numata, A. Kemery, and J. Camp, *Phys. Rev. Lett.* **93**, 250602 (2004).
- [7] K. Pyragas, *Phys. Lett. A* **170**, 421 (1992).
- [8] J. E. S. Socolar, D. W. Sukow, and D. J. Gauthier, *Phys. Rev. E* **50**, 3245 (1994).
- [9] D. W. Sukow, M. E. Bleich, D. J. Gauthier, and J. E. S. Socolar, *Chaos* **7**, 560 (1997).
- [10] A. G. Balanov, N. B. Janson, and E. Schöll, *Phys. Rev. E* **71**, 016222 (2005).
- [11] D. Goldobin, M. Rosenblum, and A. Pikovsky, *Phys. Rev. E* **67**, 061119 (2003).
- [12] N. B. Janson, A. G. Balanov, and E. Schöll, *Phys. Rev. Lett.* **93**, 010601 (2004).
- [13] P. Hövel and E. Schöll, *Phys. Rev. E* **72**, 046203 (2005).
- [14] W. Lu and R. G. Harrison, *Opt. Commun.* **109**, 457 (1994).
- [15] C. Simmendinger and O. Hess, *Phys. Lett. A* **216**, 97 (1996).
- [16] Y. Liu and J. Ohtsubo, *IEEE J. Quantum Electron.* **33**(7), 1163 (1997).
- [17] S. Bauer, O. Brox, J. Kreissl, B. Sartorius, M. Radziunas, J. Sieber, H. J. Wunsche, and F. Henneberger, *Phys. Rev. E* **69**, 016206 (2004).
- [18] R. Lang and K. Kobayashi, *IEEE J. Quantum Electron.* **16**, 347 (1980).
- [19] B. Haegeman, K. Engelborghs, D. Roose, D. Pieroux, and T. Erneux, *Phys. Rev. E* **66**, 046216 (2002).
- [20] M. Wolfrum and D. Turaev, *Opt. Commun.* **212**, 127 (2002).
- [21] K. Engelborghs, T. Luzyanina, and G. Samaey, *DDE-BIFTOOL v. 2.00: A MATLAB package for bifurcation analysis of delay differential equations*, Technical Report TW-330, Department of Computer Science, K.U.Leuven, Leuven, Belgium, 2001.
- [22] G. P. Agrawal and N. K. Dutta, *Semiconductor Lasers*, 2nd ed. (van Nostrand Reinhold, New York, 1993).